Advanced Powder Technology 24 (2013) 575–584

Contents lists available at SciVerse ScienceDirect

Advanced Powder Technology

journal homepage: www.elsevier.com/locate/apt

Original Research Paper

Numerical simulation of microparticles transport in a concentric annulus by Lattice Boltzmann Method

H. Hassanzadeh Afrouzi, M. Farhadi *, A. Abouei Mehrizi

Faculty of Mechanical Engineering, Babol University of Technology, Babol, P.O. Box 484, Islamic Republic of Iran

ARTICLE INFO

Article history:
Received 1 September 2012
Received in revised form 24 October 2012
Accepted 26 October 2012
Available online 22 November 2012

Keywords:
Aerosol particles
Dispersion
Removal
Brownian motion
Concentric annulus

ABSTRACT

Dispersion and removal of microaerosol particles are investigated numerically in a horizontal concentric annulus by Lattice Boltzmann Method and Lagrangian Runge–Kutta procedure with the assumption of one-way coupling. Drag, buoyancy, gravity, shear lift, Brownian motion and thermophoretic are forces that are included in particle equation of motion. All simulations were performed at Rayleigh number of 10^4 and particles specific density of 1000. The effect of aspect ratio and particles diameter were determined on particles behavior such as removal and dispersion. Results show that recirculation power increases by decreasing of cylinders gap. Particles move in a thinner quasi-equilibrium region by increasing of their diameter and decreasing of cylinders gap. Brownian motion is dominant removal mechanism in particle with diameter of 1 μm.

1. Introduction

Understanding and quantifying the behavior of particles such as deposition, aggregation and sedimentation is important in various sectors of science and technology. Some examples are the deposition of particles in channels and pipes, radioactive aerosol sampling and microcontamination control. Water purification [1], particles transport in human respiratory [2,3] and dispersion of pollution [4], determination of indoor air quality [5] are some others in biological and environmental systems. A numerical approach was developed by Li and Ahmadi [6] for transport of suspended small particles. Available experimental data's were reviewed by McCoy and Hanratty [7]. Golovin and Putnam [8] investigated the efficiency of a ribbon in a potential flow field. Phenomena of solid particle deposition on channel walls for different flow conditions were studied by Vasak et al. [9]. In recent years, the upcoming problems concerning environmental pollution have driven research efforts in different aspects of safety. One of the major issues in a severe accident scenario is to accurate prediction of the deposition rate and the removal mechanisms of microsize aerosol particles in buoyancy driven flows inside containments. Akbar et al. [10] studied the behavior of sub-micron particles in a laminar free convection in a square enclosure. Their major finding was that thermophoretic force and Brownian diffusions are the most efficient mechanisms that rule the removal process of sub-micron particles. A numerical investigation was performed by Golkarfard et al. [11] to study the transport and deposition of aerosol particles in laminar mixed-convection flow in a lid-driven cavity with two heated obstacles. They studied the effects of thermophoresis and free convection on deposition of particles on the obstacles. Their result showed that thermophoresis decreases the deposition. Puragliesi et al. [12] investigated particle deposition in the turbulent buoyancy driven flow of the differentially heated cavity (DHC). They used Direct Numerical Simulation (DNS) to simulate flow and the Lagrangian approach for calculations of dispersed phase. Their results indicated that the largest influence to particle deposition is caused by gravity effect. Deposition took place mostly at the bottom wall. They discussed in detail, contribution of lift and thermophoretic forces on particle removal. Their results showed that the lift force is responsible of particle deposition on the cold surface. It is very important to reach the accurate characteristics of flow field at particle position to calculate the Lagrangian particle tracking procedure. The Lattice Boltzmann Method (LBM) is a suitable numerical technique based on kinetic theory for simulating fluid flows and modeling the physics in fluids especially in bounded boundary [13–17].

The annular shape enclosure is one of the most applicable geometry in engineering and industry, the geometry of the horizontal circular annulus is commonly found in solar collector-receiver, underground electric transmission cables, and vapor condenser for water distillation, heat exchangers and food process. Kuehn and Goldstein [18,19] accomplished and reviewed the most reliable studies about the free convection in annulus.

* Corresponding author. Tel.: +98 111 3234205; fax: +98 111 3212268.
E-mail addresses: h.h.afrouzi@stu.nit.ac.ir (H.H. Afrouzi), mfarhadi@nit.ac.ir (M. Farhadi), abbasabouei@gmail.com (A.A. Mehrizi).

0921-8831/$ - see front matter © 2012 The Society of Powder Technology Japan. Published by Elsevier B.V. and The Society of Powder Technology Japan. All rights reserved.
http://dx.doi.org/10.1016/j.apt.2012.10.006

Nomenclature

AR	aspect ratio
C_c	Cunningham correction factor
c_k	discrete lattice velocity in direction (k)
c_s	speed of sound in lattice scale
DPF	deposited particle fraction
d^p	particle diameter (μm)
F_k	external force in direction of lattice velocity
f_k^{eq}	equilibrium distribution function
g	gravity (m/s^2)
G	Gaussian random number
Gr	Grashof number
$H = Ro - Ri$	length scale
k	thermal conductivity (w/m k)
$kn_p = 2\lambda/d^p$	particle Knudsen number
K_{Th}	thermophoretic coefficient
L	Saffman lift force (N/kg)
MSV	maximum stream function value
N_P	number of particles
N	Brownian force (N/kg)
$\Pr = \nu/\alpha$	Prandtl number
$Ra = g\beta\Delta TH^3/\alpha\upsilon$	Rayleigh number
r	Radial coordinate
Ri	inner radius
Ro	outer radius
$S = \rho^p/\rho^g$	particle Specific density
SPF	suspended particle fraction
Th	thermophoretic force (N/kg)
Tf	final time
T	temperature
u	horizontal components of velocity (m/s)
v	vertical components of velocity (m/s)

Greek symbols

β	thermal expansion coefficient (1/k)
ρ	density (kg/m^3)
τ	lattice relaxation time
$\tau_p = \frac{\rho^p c_c (d^p)^2}{18\mu}$	particle relaxation time (s)
Δt	lattice time step
ν	kinematic viscosity (m^2/s)
λ	gas mean free path (μm)

Subscripts

c	cold
h	hot
Th	thermophoretic
p	particle
g	gas

Superscript

i	vector axis indicators

The objective of the present study is to determine the effect of aspect ratio of annulus and particles diameter on the particles removal and dispersion. The Lattice Boltzmann Method is used to simulate laminar flow in a concentric annulus. Then particle equation of motion is solved to investigate dispersion and removal of particles. Drag, Saffman lift, gravity, buoyancy, Brownian motion and thermophoretic are forces that included in Lagrangian particle tracing procedure.

2. Lattice Boltzmann Method

The general form of Lattice Boltzmann equation with external force can be written as:

$$f_k(\vec{x}+\vec{c}_k\Delta t, t+\Delta t) - f_k(\vec{x},t) = \Delta t \frac{f_k^{eq}(\vec{x},t) - f_k(\vec{x},t)}{\tau} + \Delta t \cdot \vec{F} \tag{1}$$

where Δt is lattice time step, $\vec{c}_k$ is the lattice velocity in direction k, F_k is the is the particle distribution function which corresponds to the external force in direction of $\vec{c}_k$ and τ denotes the lattice relaxation time and it is defined as:

$$\tau = \left(\frac{1}{\Delta t c_s^2}\right)\upsilon + 1/2 \tag{2}$$

where υ is the kinematic viscosity. f_k^{eq} is the equilibrium distribution function and depends on on the type of problem. The equilibrium distribution functions for fluid field are calculated with following equation:

$$f_k^{eq} = \omega_k \cdot \rho \left[1 + \frac{\vec{c}_k \cdot \vec{u}}{c_s^2} + \frac{1}{2}\frac{(\vec{c}_k \cdot \vec{u})^2}{c_s^4} - \frac{1}{2}\frac{\vec{u}\cdot\vec{u}}{c_s^2}\right] \tag{3}$$

where ρ and $\vec{u}$ are the macroscopic fluid density and velocity and are calculated as below:

$$\text{Flow density} : \rho = \sum_k f_k \tag{4}$$

$$\text{Momentum} : \rho\vec{u} = \sum_k f_k \vec{c}_k \tag{5}$$

ω_k are weighting factors. The values of $w_0 = 4/9$ for $|c_0| = 0$, $w_{1-4} = 1/9$ for $|c_{1-4}| = 1$ and $w_{5-8} = 1/36$ for $|c_{5-8}| = \sqrt{2}$ are assigned in this model. The thermal Lattice Boltzmann equation could be written as below:

$$g_k(\vec{x}, t+\Delta t) - g_k(\vec{x},t) = \Delta t \frac{g_k^{eq}(\vec{x},t) - g_k(\vec{x},t)}{\tau_c} \tag{6}$$

where the thermal equilibrium distribution functions are given as:

$$g_k^{eq} = \omega_k T\left[1 + \frac{\vec{c}_k \cdot \vec{u}}{c_s^2}\right] \tag{7}$$

T is the fluid temperature and evaluated from:

$$T = \sum_k g_k^{eq} \tag{8}$$

The temperature relaxation time is calculated as a function of diffusivity coefficient:

$$\tau_c = \left(\frac{1}{\Delta t c_s^2}\right)\alpha + 1/2 \tag{9}$$

In order to incorporate buoyancy force in the model, the Boussinesq approximation was applied, therefore the force term in the Eq. (1) need to be calculated as below in vertical direction (y):

$$\vec{F}_y = 3\omega_k \vec{g}_y \beta \Delta T \tag{10}$$

where $\vec{g}_y$ is the acceleration of gravity acting in the y-direction of the lattice links; β is the thermal expansion coefficient and ΔT is temperature difference.

2.1. Curved boundary treatment

In the present study, a second-order accurate method to define curve boundary condition is used [20]. Fig. 1 shows the lattice node

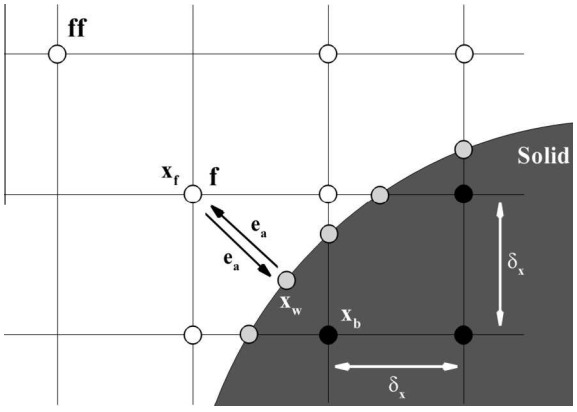

Fig. 1. Layout of the regularly spaced lattices and curved wall boundary.

treatment on curved boundary condition, the solid block nodes indicates the boundary nodes x_b, the white nods shows the first fluid nodes x_f and the gray nodes on the boundary x_w indicates the intersections of the wall with various lattice links.

The fraction of an intersected link in the fluid region Δ, is determined by:

$$\Delta = \frac{|x_f - x_w|}{|x_f - x_b|} \tag{11}$$

At the collision step, the fluid side distribution function on the fluid side $\tilde{f}_k$, is determined but the solid side distribution function at the opposite direction $\tilde{f}_{\bar{k}}$, is unknown. On the other hand to finish the streaming step, we need to know $\tilde{f}_{\bar{k}}$ at the boundary node x_b. More detail about the velocity and temperature boundary conditions over the curved body can be found at the study of Fattahi et al. [15].

3. Dispersed phase

A particle suspended in buoyancy driven flow is affected by some forces. Drag, Saffman lift, gravity, buoyancy, Brownian motion and thermophoretic are included in particle equation of motion in this study. The corresponding particle equation of motion in i direction is given as:

$$\frac{du_p^i}{dx^i} = \frac{1}{\tau_p}(u_g^i - u_p^i) + L^i + N^i + \left(1 - \frac{1}{S}\right)g^i + Th^i \tag{12}$$

The first term in right hand side of Eq. (12) is drag force that is due to relative velocity between particles and carrier gas. The relaxation time τ_p is the characteristic time scale (response time) of particle. The particle needs to this time to response the variation of flow field. u_p^i and u_g^i are the corresponding particle and velocity indirection of i. S is specific gravity, m^p is the particle mass and g^i is gravity acceleration. By increasing the relaxation time, particle reaction decreases to variation of flow parameters. For submicron particles with particle Knudsen number $kn_p = \frac{2\lambda}{d^p}$ greater than 0.1, when the particle diameter is in the range of gas mean free path (λ), flow slips over the particle surface. Therefore, the Stokes drag must be modified by Cunningham correction factor (C_c) as [21]:

$$C_c = 1 + \frac{2\lambda}{d_p}\left[1.257 + 0.4e^{\left(\frac{-1.1d_p}{2\gamma_g}\right)}\right] \tag{13}$$

Small particles in a shear field experience a force perpendicular to the direction of flow. The shear lift originates from the inertia effects in the viscous flow around the particle and is different from aerodynamic lift force that originates from shape asymmetry of particles. The first equation for this force was obtained by Saffman [22]:

$$L^i = \frac{2k_L v^{0.5} d_{ij}}{S d_p (d_{lk} d_{kl})}(u_g^i - u_p^i) \tag{14}$$

ρ^p and v are density and kinematic viscosity of gas phase, respectively. $k = 2.549$ is constant coefficient of Saffman lift force and d_{ij} is deformation tensor and define as [21]:

$$d_{ij} = \frac{1}{2}(u_{i,j} + u_{j,i}) \tag{15}$$

Finally, the Brownian motion per unit mass in direction i is denoted by N^i. The instantaneous random momentum that imparts to the ultrafine particles due to the impaction of the gas molecules, which causes the particle to move on an erotic path known as Brownian motion [21,23]:

$$N^i = G\sqrt{\frac{\pi S_0}{\Delta t}} \tag{16}$$

$$S_0 = \frac{216 v K_1 T_g}{\pi^2 \rho_p (d_p)^5 S^2 C_c} \tag{17}$$

T_g is gas temperature and $K_1 = 1.38 \times 10^{-23}\,\frac{j}{k}$. G is unit variance zero mean Gaussian random numbers as:

$$G = \sqrt{-2\ln U_i}\cos(2\pi U_j) \tag{18}$$

where U^i and U^j are random numbers (between 0 and 1). Finally, Th^i denotes thermophoretic force which is defined as:

$$Th = K_{Th}\frac{\partial T}{\partial x^i} \tag{19}$$

where K is the thermophoretic coefficient suggested by Talbot et al. [24]:

$$K_{Th} = \frac{2C_s C_c\left[\left(\frac{K_g}{K_p}\right) + C_t K n_p\right]}{(1 + 3C_m K n_p)(1 + 2\frac{K_f}{K_p} + 2C_t K n_p)} \tag{20}$$

The values of C_t, C_m and C_s are 2.18, 1.14 and 1.17, respectively [25]. The K_f and K_p are the thermal conductivity of fluid and particle, respectively. By solving particle equation of motion for particles, particles path is obtained by:

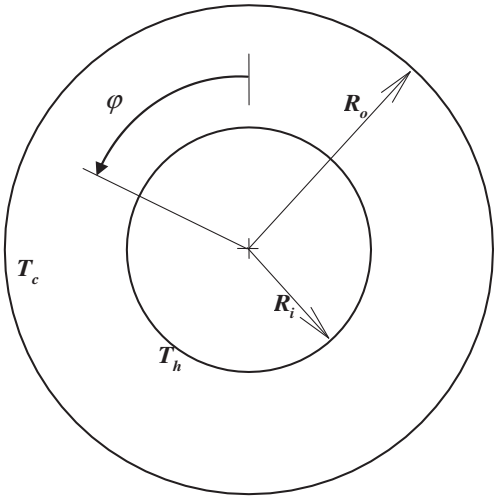

Fig. 2. Computational domain of concentric annulus.

Table 1
Annulus characteristic at Ra = 10^4, ΔT and R_o = 0.5 (cm).

Aspect ratio (AR)	Inner cylinder diameter (cm)
2	0.25
3	0.167
4	0.125

$$\frac{dx^i}{dt} = u_p^i \tag{21}$$

4. Numerical procedure

In the present study an in-house code is developed to use hybrid Lattice Boltzmann Method and discrete phase model for simulating flow characteristics and particle trajectories in the buoyancy driven natural convection laminar flow. Computational domain is considered a two dimensional concentric cylindrical annulus with inner radius R_i and outer radius R_o (Fig. 2). The 200×200 grid resolution is used to perform the simulation.

The aspect ratio is defined as the ratio of outer radius to the inner radius. The cylinder surfaces are maintained at two different uniform temperatures. The Rayleigh number Eq. (22) is fixed at 10^4:

$$\mathrm{Ra} = \frac{g\beta\Delta T H^3}{\nu_g \alpha_g} \tag{22}$$

When the flow reached to the steady state, with the flow velocity distribution known, tracking of random distributed particles are then performed in a Lagrangian frame with assumption of one-way coupling. In the one way coupling assumption, Particles do not impart momentum to the carrying fluid and also there is no collision of particles. These effects are considered for high particles concentration [26]. It is necessary to convert the all lattice parameters to real ones to use them in the particle equation of motion. It is due to presence of dimensional parameters in the equation of motion. For example with equality of Fourier number as dimensionless time of LBM results and real condition, the relation of real time and Lattice time step obtained as:

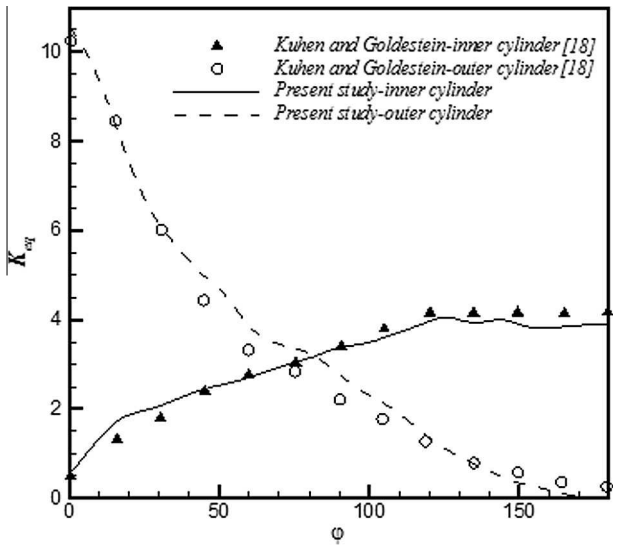

Fig. 4. Comparison of equivalent thermal conductivity on inner and outer cylinder with experimental results of Kuehn and Goldstein [18] for annulus at Ra = 5×10^4.

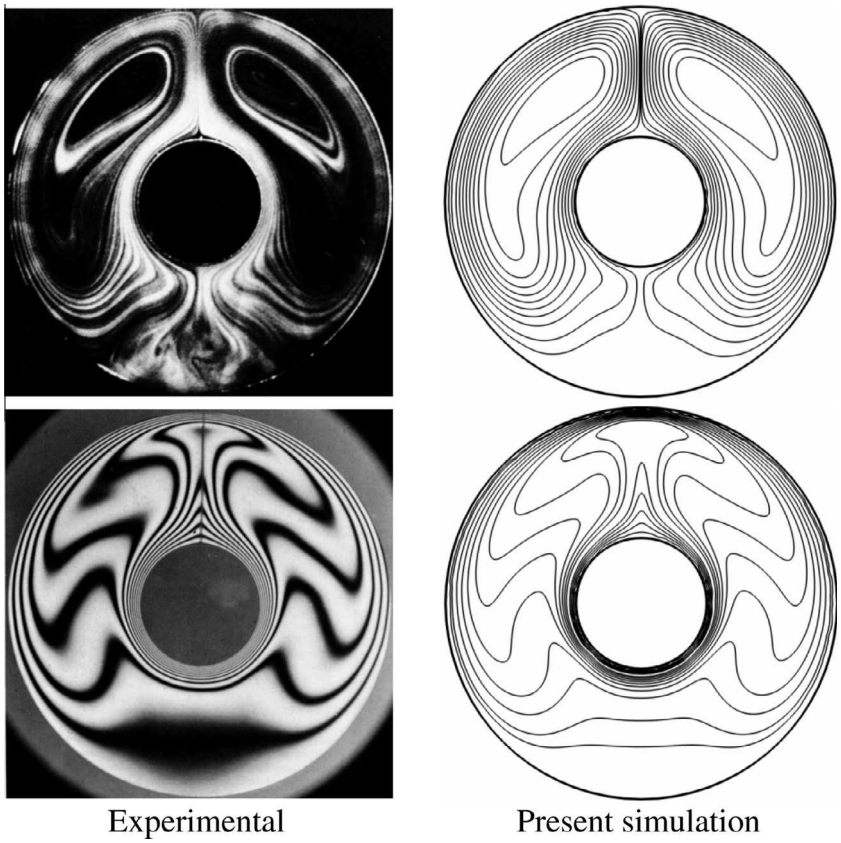

Fig. 3. Comparison with experimental result of Grigull and Hauf [27]. The streamlines for Gr = 120,000 (top) and Isotherms for Gr = 122,000 (bottom).

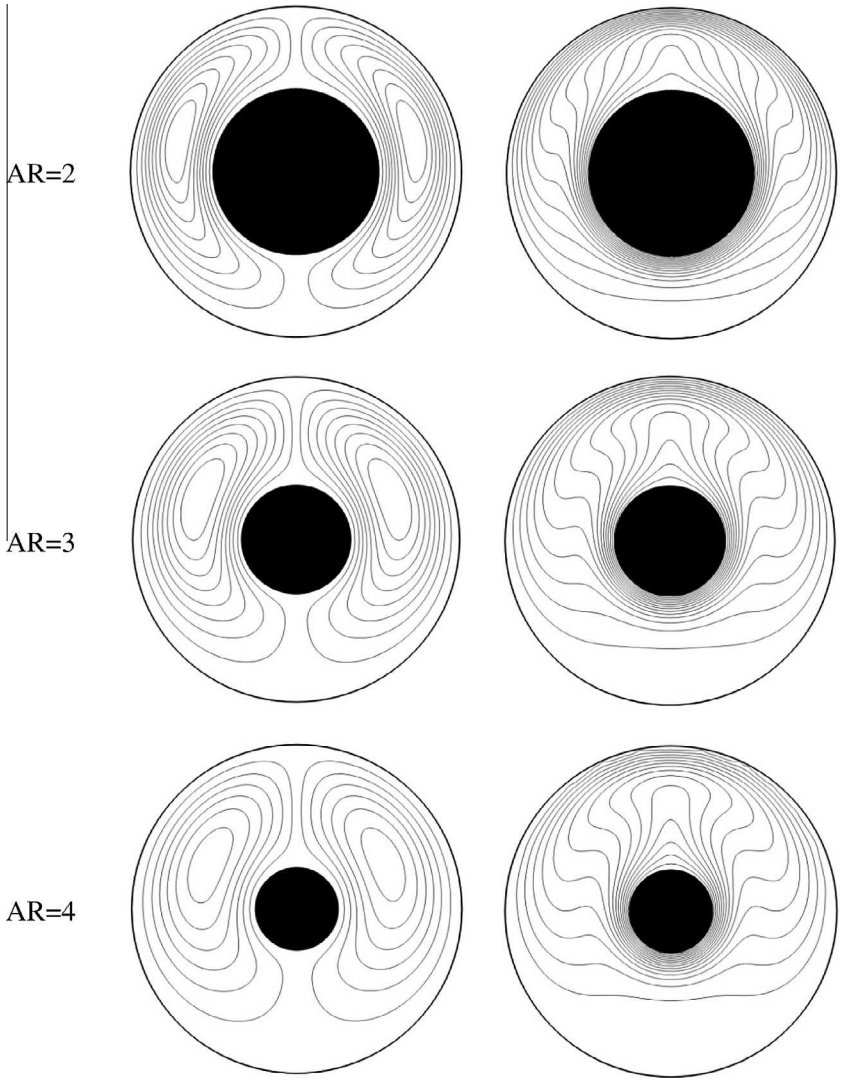

Fig. 5. The streamlines (right) and isotherms (left) at Ra = 10^4.

Table 2
Annulus Maximum stream function value versus aspect ratio at Ra = 10^4.

Aspect ratio (AR)	MSV
2	3.97
3	3.31
4	2.96

$$t_{(Red)} = t_{(Lattice)} \times \frac{\alpha_{(Lattice)}}{\alpha_{(Red)}} \times \frac{H^2}{N^2} \tag{23}$$

Particles trajectories are studied at different aspect ratio (AR). The particle initial slip velocity is set to zero and the temperature of particles is assumed by a linear distribution between the cold and the hot walls temperature. This assumption is employed to obtain particles properties. The characteristics of annulus are presented in Table 1. Particles are selected with different diameter at $S = 1000$ to obtain a wide range of microsize aerosol behavior.

Standard 4th-order explicit Runge–Kutta (ERK4) method is implemented in order to time integrates the particles trajectory. Consider the first order ODE:

$$\frac{dy}{dx} = f(x, y) \tag{24}$$

The formula for 4th order Runge–Kutta approximation to the above ODE is given as:

$$y_{n+1} = y_n + \frac{h}{6}(K_1 + 2(K_2 + K_3) + K_4) + O(h^5) \tag{25}$$

where:

$$\begin{aligned} K_1 &= f(x_n, y_n) \\ K_2 &= f\left(x_n + \frac{h}{2}, y_n + h\frac{K_1}{2}\right) \\ K_3 &= f\left(x_n + \frac{h}{2}, y_n + h\frac{K_2}{2}\right) \\ K_4 &= f\left(x_n + \frac{h}{2}, y_n + hK_3\right) \end{aligned} \tag{26}$$

Perfect absorbing wall condition is assumed at the wall boundaries. This implies that when particles distance with cylinders surfaces becomes smaller than radius of particles they stick to cylinders and do not reenter in the flow domain because of rebounce or lubrication effects. In the particle calculations the Δt was 10^{-5} at all cases. Since the effect of randomness may become important in the simulation of Brownian force, simulation of some cases with $d_p = 1$ μm are performed with different time steps to ensure that calculations are independent of time step.

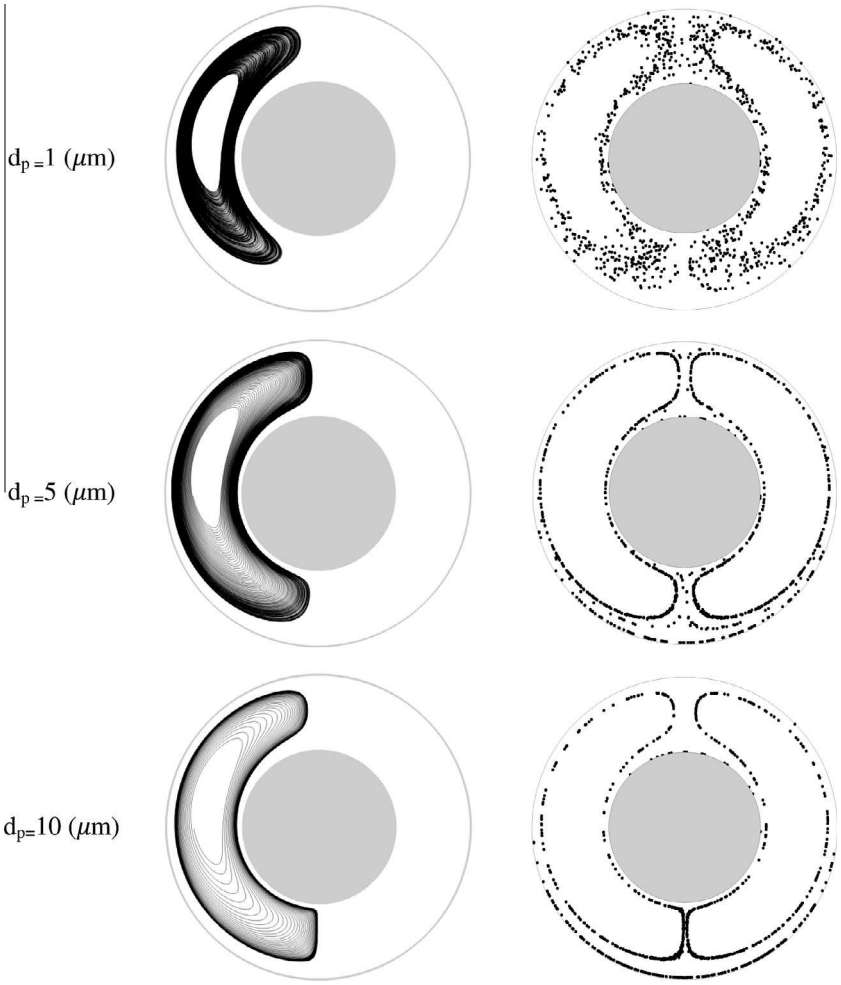

Fig. 6. A particle trajectories (left) and all particles end positions (right) at AR = 2.

5. Result and discussion

The present study considers two horizontal circular cylinder of inner and outer radius, R_i and R_o, respectively. A temperature difference is applied with subjecting the walls of the inner cylinder to a higher temperature (T_h) than its outer cylinder counterpart (T_c). The effect of aspect ratio and particles diameter are investigated on aerosol particles behavior. An experimental study is selected to validate flow field and isotherms. Gr number of 120000 and 122000 are selected to compare streamlines and isotherms of present simulation with experimental results of Grigull and Hauf [27]. Results show agreement between the present computations and their experiments as shown in Fig. 3. For furthermore validation, the local equivalent thermal conductivity is obtained. Results have been compared with the study of Kuehn and Goldstein [18]. This parameter is defined as the actual heat flux divided by the heat flux that would be occurred by pure conduction in the absence of fluid motion. Results of local equivalent thermal conductivity are shown in Fig. 4 and represent good agreement between the present computations and their experiments results. In particular, the present local equivalent thermal conductivity results are well within ±3% of the benchmark data by Kuehn and Goldstein [18]. The streamlines and isotherms are presented for aspect ratio of 2, 3 and 4 at $Ra = 10^4$ in Fig. 5. Two large recirculation areas form between cylinders at the left and right sides. The flow moves clockwise in the right section of annulus. It is due to the inner wall push flow to the top of the annulus and cold outer wall push it downward. Finally flow moves counterclockwise in the left section of annulus On the basis of same reason.

Variation of aspect ratio effects on flow field and heat transfer characteristics. At, smaller aspect ratio (AR = 2), buoyancy driven flow is limited to circulate in a smaller region. So the buoyancy power is great. By increasing the aspect ratio to 3 and 4, the speed (strength) of recirculation zones decreases. It is clear in the behavior of maximum Stream function value at different aspect ratios (Table 2).

5.1. Particles dispersion and removal

The particle with sizes in the range of 1–10 μm at $S = 1000$ are selected for simulating. Drag, Saffman lift, gravity, buoyancy, Brownian motion and thermophoretic are forces that included in particle equation of motion. The effect of aspect ratio and particles diameter are investigated on the particles behavior such as removal and dispersion. Hydrodynamic force, gravity and inertia of particles are primary contributors in the microparticles dynamic. Since the flow velocity vectors are changing sharply, relative velocity between carrier (gas) and discrete phases (particle), causes slip between particles and gas molecules to develop. The flow passes through curve lines in annulus and particles cannot follow it exactly that is due to inertial force. Particles which are near the solid boundaries, contact with walls and are captured there. This behavior is called inertial impaction.

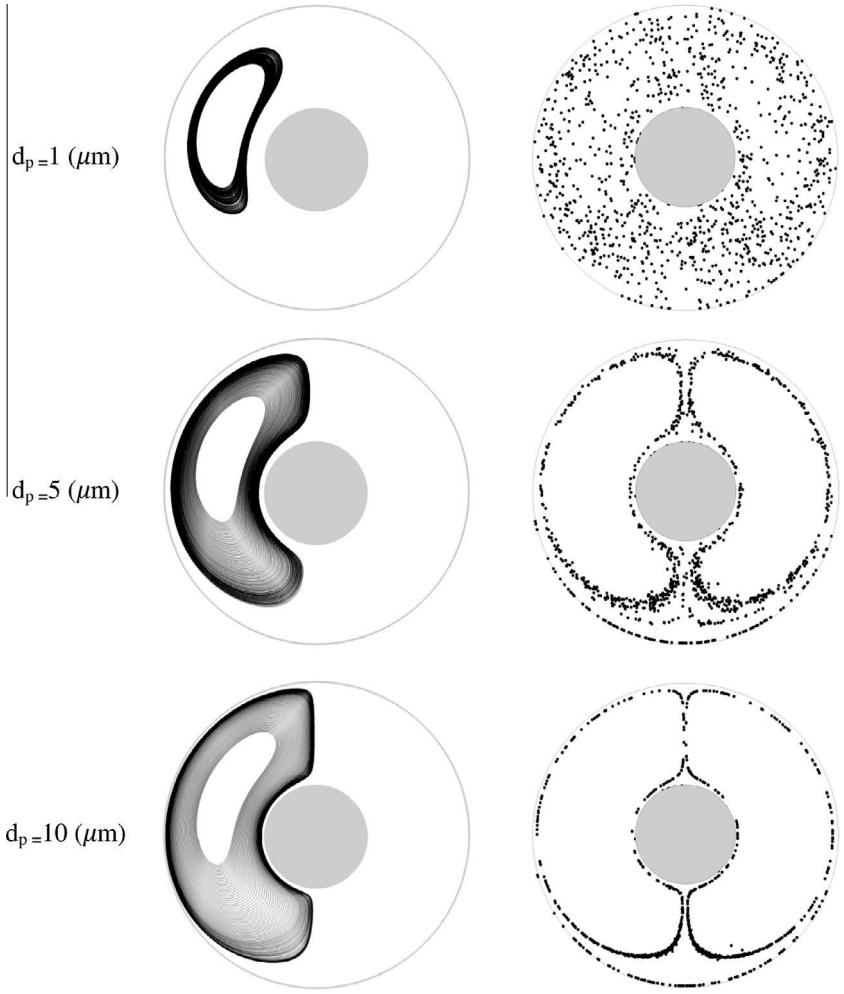

Fig. 7. A particle trajectories (left) and all particles end positions (right) at AR = 3.

This phenomenon is more sensible for heavy particles. Brownian motion is dominant removal mechanism for ultrafine particles with diameter less than 1 (μm). However, Brownian motion comes into account for particles with diameter in the range of present simulation.

A specific particle trajectory and all particles end positions with diameter of 1, 5 and 10 micrometer are presented for different aspect ratios at Ra = 10^4 in Figs. 6–8. Hydrodynamic forces of the two recirculation regions tend to hold the particles in themselves and Inertia force pushes the particles outward. Finer particles are caught up in the recirculating flow and remain suspended in the gas in two quasi-equilibrium zones at both right and left sides of annulus. It is due to the outward and inward forces are nearly balanced. As particles diameter increases, the inertial force causes particles to deviate from inner streamlines to outers. So quasi-equilibrium zones form in a thinner bounded curve near the cylinder surfaces. By increasing the aspect ratio to 3 and 4, recirculation power decreases (Table 2). So particles acceleration and their inertia decreases and quasi-equilibrium zones become thicker and cover the large part of flow. It should be mentioned that hydrodynamic forces decrease too.

The progress of particles dispersion is shown over the time in Fig. 9. Figures provide the instantaneous snapshots of particles locations for the two different sets (d_p = 3 μm, d_p = 6 μm) and the two aspect ratio AR = 2, 3 at time t = 1, 10, 50. Figure indicates that particles reach the quasi equilibrium region at aspect ratio (AR) of 2 in a shorter time with respect to AR = 3 (red[1] and green dots). It means that particle disperses in a quasi-steady state in first few seconds.

Time histories of particles removal fraction (PRF) for particles with three different diameters are presented in Fig. 10 at different aspect ratios. For particles with medium (d_p = 5 μm) and large (d_p = 10 μm) sizes PRF shows three different time behaviors clearly: during the first few seconds, high and almost linear trends (constant rate) are observed in PRF. It is due to the initial velocity of particles are set zero. So the effect of gravitation plays the important role in the deposition process. As time passes, increasing of particles velocity reduces this effect in later seconds. The instant when the removal rate changes sharply and become almost horizontal, are proportional to the time needed by most number of particles that will be deposited, to remove from the equilibrium regions. For medium and large Particles also, removal process takes less time by increasing of particle diameters. It is due to the effect of gravity that helps inertia to enforce particles deviate from their streamlines to move from inner streamlines to outer ones in the recirculation region and hit the wall in a shorter time. As aspect ratio increases, particles removal fraction (PRF) reaches its maximum value in a longer time. In fact particle must cover larger distance to hit the wall as the gap of cylinders become greater.

[1] For interpretation of color in Fig. 9, the reader is referred to the web version of this article.

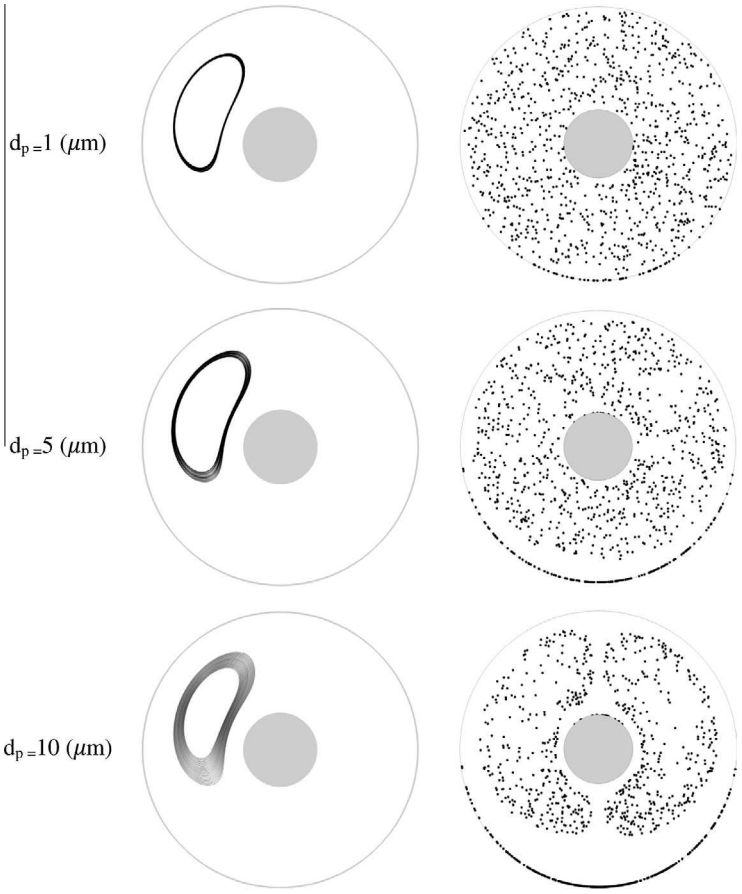

Fig. 8. A particle trajectories (left) and all particles end positions (right) at AR = 4.

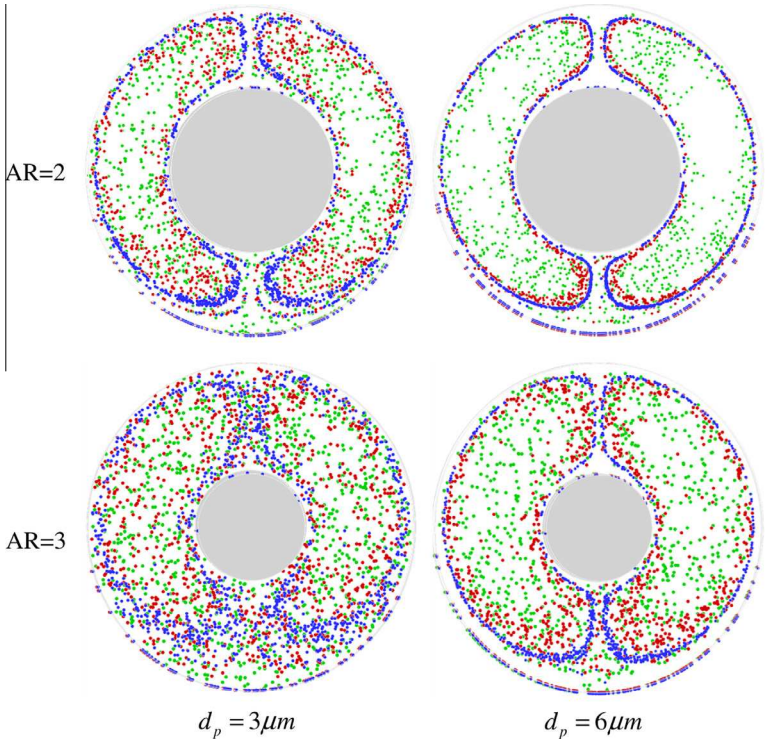

Fig. 9. Three instantaneous snapshots of particle locations at seconds of t = 1 s (green), 5 s (red), 50 s (blue). On the left column the case for d_p = 3 μm, on the right the case for d_p = 6 μm.

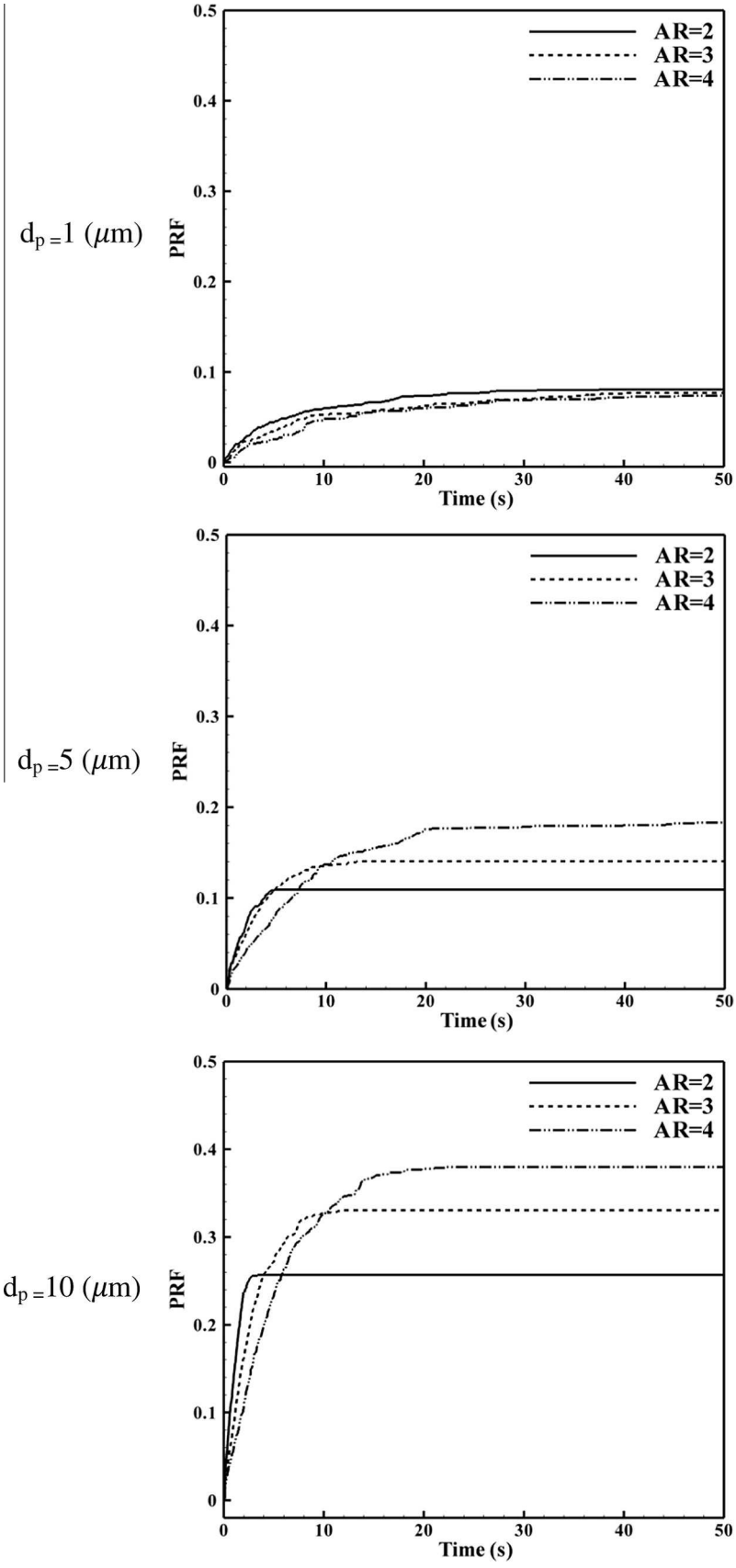

Fig. 10. Time histories of deposited particle fraction.

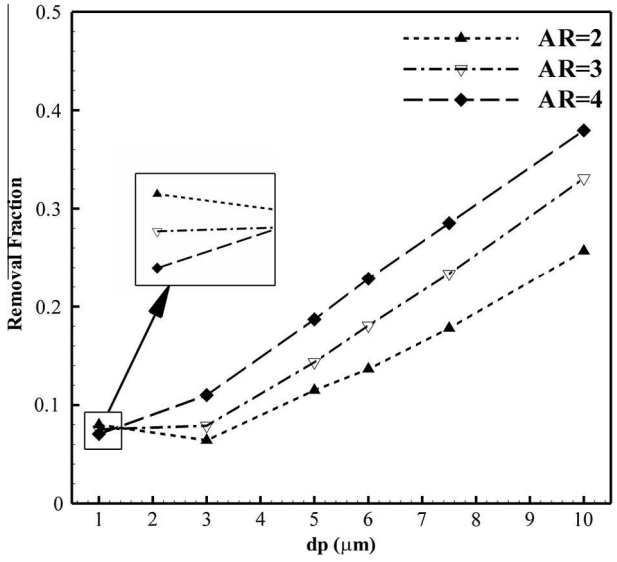

Fig. 11. Particles removal fraction at different aspect ratio (Ar).

The first linear and high removal rate region is not obvious for the smallest simulated particles (1 μm). It is clear that the small particles in the cores are much more influenced by the hydrodynamic force and their quasi-equilibrium regions are larger. Brownian motion also, causes removal process to take much time. It is due to the deviation of particles from moving on the streamlines. Gravitation also, is not significant for this particle. This yields the linear trend to vanish.

Fig. 11 shows that, particles removal increases at greater aspect ratios in constant particles diameter because of the hydrodynamic decreasing effect against the effect of gravity except for particle with diameter of 1 (μm). Bold region of curve shows the removal of particles decreases with the increase in the aspect ratio. As indicated before, forming of quasi-equilibrium zones near the surfaces causes that a number of random moving particles come in contact with surfaces and deposit.

6. Conclusion

In the present study Lattice Boltzmann Method is used to simulate natural convection flow in a concentric annulus. Runge–Kutta is implemented to calculate particle trajectories. All simulations were performed at Rayleigh number of 10^4 and particles specific density of 1000. Two experimental studies were selected to validate flow field and thermal characteristic of natural convection and results show excellent agreement with them. The effect of cylinders gap and particles size are investigated on removal and dispersion of particles. As aspect ratio increases, the strength of recirculation regions and maximum stream-function value augments. As particles diameter increases the quasi equilibrium zones that particles move on, become thinner and locate in vicinity of cylinders surfaces. This phenomenon occurs by decreasing of aspect ratio. Particles removal increases as cylinders gap decreases. Brownian motion is dominant removal mechanism in particle with diameter of 1 μm.

References

[1] R.D. Ambashta, M. Sillanpää, Water purification using magnetic assistance. A review, Journal of Hazardous Materials 180 (2010) 38–49.
[2] J. Huang, L. Zhang, Numerical simulation of micro-particle deposition in a realistic human upper respiratory tract model during transient breathing cycle, Particuology 9 (2011) 424–431.
[3] J. Heyder, J. Gebhart, G. Rudolf, C.F. Schiller, W. Stahlhofen, Deposition of particles in the human respiratory tract in the size range 0.005–15 μm, Journal of Aerosol Science 17 (1986) 811–825.
[4] M. Ketzel, R. Berkowicz, Multi-plume aerosol dynamics and transport model for urban scale particle pollution, Atmospheric Environment 39 (2005) 3407–3420.
[5] F. Chen, S.C.M. Yu, A.C.K. Lai, Modeling particle distribution and deposition in indoor environments with a new drift–flux model, Atmospheric Environment 40 (2006) 357–367.
[6] A. Li, G. Ahmadi, Aerosol particle deposition with electrostatic attraction in a turbulent channel flow, Journal of Colloid and Interface Science 158 (1993) 476–482.
[7] D. McCoy, T. Hanratty, Rate of deposition of droplets in annular two-phase flow, International Journal of Multiphase Flow 3 (1977) 319–331.
[8] M. Golovin, A. Putnam, Inertial impaction on single elements, Industrial and Engineering Chemistry Fundamentals 1 (1962) 264–273.
[9] F. Vasak, B. Bowen, C. Chen, F. Kastanek, N. Epstein, Fine particle deposition in laminar and turbulent flows, Canadian Journal of Chemical Engineering 73 (1995) 785–792.
[10] M.K. Akbar, M. Rahman, S.M. Ghiaasiaan, Particle transport in a small square enclosure in laminar natural convection, Journal of Aerosol Science 40 (2009) 747–761.
[11] V. Golkarfard, S.A. Gandjalikhan Nasab, A.B. Ansari, G.H. Bagheri, Numerical investigation on deposition of solid particles in a lid-driven square cavity with inner heated obstacles, Advanced Powder Technology, in press.
[12] R. Puragliesi, A. Dehbi, E. Leriche, A. Soldati, M.O. Deville, DNS of buoyancy-driven flows and Lagrangian particle tracking in a square cavity at high Rayleigh numbers, International Journal of Heat and Fluid Flow 32 (2011) 915–931.
[13] X. Nie, G.D. Doolen, S. Chen, Lattice-Boltzmann simulations of fluid flows in MEMS, Journal of Statistical Physics 107 (2002) 279–289.
[14] X. He, S. Chen, R. Zhang, A lattice Boltzmann scheme for incompressible multiphase flow and its application in simulation of Rayleigh–Taylor instability, Journal of Computational Physics 152 (1999) 642–663.
[15] E. Fattahi, M. Farhadi, K. Sedighi, Lattice Boltzmann simulation of natural convection heat transfer in eccentric annulus, International Journal of Thermal Sciences 49 (2010) 2353–2362.
[16] M.A. Delavar, M. Farhadi, K. Sedighi, Numerical simulation of direct methanol fuel cells using lattice Boltzmann method, International Journal of Hydrogen Energy 35 (2010) 9306–9317.
[17] S. Ansumali, I. Karlin, C.E. Frouzakis, K. Boulouchos, Entropic lattice Boltzmann method for microflows, Physica A: Statistical Mechanics and its Applications 359 (2006) 289–305.
[18] T. Kuehn, R. Goldstein, An experimental and theoretical study of natural convection in the annulus between horizontal concentric cylinders, Journal of Fluid Mechanics 74 (1976) 695–719.
[19] T. Kuehn, R. Goldstein, An experimental study of natural convection heat transfer in concentric and eccentric horizontal cylindrical annuli, Journal of Heat Transfer 100 (1978) 635.
[20] R. Mei, L.-S. Luo, W. Shyy, An accurate curved boundary treatment in the lattice Boltzmann method, Journal of Computational Physics 155 (1999) 307–330.
[21] M. Shams, G. Ahmadi, H. Rahimzadeh, A sublayer model for deposition of nano- and micro-particles in turbulent flows, Chemical Engineering Science 55 (2000) 6097–6107.
[22] P.G. Saffman, The lift on a small sphere in a slow shear flow, Journal of Fluid Mechanics 22 (1965) 385–400.
[23] A. Li, G. Ahmadi, Dispersion and deposition of spherical particles from point sources in a turbulent channel flow, Aerosol Science and Technology 16 (1992) 209–226.
[24] L. Talbot, R. Cheng, R. Schefer, D. Willis, Thermophoresis of particles in a heated boundary layer, Journal of Fluid Mechanics 101 (1980) 737–758.
[25] R. Chein, W. Liao, Thermophoretic effects on nano-particle deposition in channel flow, Heat and mass transfer 42 (2005) 71–79.
[26] L. Wang, G. Zhoua, X. Wang, Q. Xionga, W. Ge, Direct numerical simulation of particle fluid systems by combining time driven hard sphere model and lattice Boltzmann method, Particuology 8 (2010) 379–382.
[27] U. Grigull, W. Hauf, Natural convection in horizontal cylindrical annuli, Proceeding of the 3rd International Heat Transfer Conference, vol. 2, 1966, pp. 182–195.